IEEE Access
Multidisciplinary | Rapid Review | Open Access Journal

Received 11 April 2024, accepted 28 May 2024, date of publication 11 June 2024, date of current version 19 June 2024.

Digital Object Identifier 10.1109/ACCESS.2024.3412242

RESEARCH ARTICLE

Robust Multi-Event Detection for Pulsed LiDARs

SEUNG SOO KWAK, (Graduate Student Member, IEEE), JISEONG LEE, (Graduate Student Member, IEEE), YUN CHAN IM, (Graduate Student Member, IEEE), HYUNJIN LEE, (Graduate Student Member, IEEE), AND YONG SIN KIM, (Senior Member, IEEE)

School of Electronic Engineering, Korea University, Seoul 02841, South Korea

Corresponding author: Yong Sin Kim (shonkim@korea.ac.kr)

This work was supported in part by the National Research Foundation of Korea (NRF) Grant funded by the Korean Government (MSIT) under Grant NRF-2021R1A2C2014652; in part by Korea Institute of Planning and Evaluation for Technology in Food, Agriculture and Forestry (IPET) through the Open Field Smart Agriculture Technology Short-Term Advancement Program, funded by the Ministry of Agriculture, Food and Rural Affairs (MAFRA) under Grant 322029032HD070; and in part by the IC Design Education Center (IDEC) for the Chip Fabrication, South Korea.

ABSTRACT Pulsed light detection and rangings (LiDARs) are widely utilized in various applications such as navigation, robotic, and remote sensing for their high distance resolution, accuracy, and speed. When multiple echoes are received either from interferences or under harsh environmental conditions, conventional pulsed LiDARs fail to extract the distance information out of received signal. To overcome this problem, this paper introduces a multi-event detecting pulsed LiDAR that delivers multiple distance and intensity information when multiple echoes are received. The proposed system comprises an analog front-end (AFE), a timing discriminator with 8 comparators, a multi-event detector, and a time-to-amplitude converter (TAC) for the timing circuit, capable of capturing the distance and intensity information up to four echoes. For quantification, experiments based on multiple echoes with multiple local peaks are conducted using an electrical model generated from real situation. Each event delivers 3-bit intensity information, and the measured distance information with a 10-bit analog-to-digital converter (ADC) exhibits the time resolution of 146.5 ps and the integral nonlinearity (INL) of 1.17 LSB.

INDEX TERMS Pulsed LiDAR, multi-event detection, multiple echoes.

I. INTRODUCTION

Light detection and ranging (LiDAR) is a distance sensor widely used in various fields such as terrain visualization, augmented vision, reconnaissance, pedestal detection, unmanned aerial vehicles (UAVs), automobile auxiliary driving, smart robots, and more [1], [2]. LiDARs can be classified into two types: continuous-wave and pulsed. Frequency modulated continuous-wave (FMCW) and amplitude modulated continuous-wave (AMCW) are two different types of continuous-wave LiDARs [3]. Pulsed LiDARs are commonly employed on modern outdoor LiDAR systems over continuous-wave LiDARs for their lower complexity, high resolution, high accuracy, and fast sampling time [4], [5]. However, the accuracy of pulsed LiDAR can severely be affected by external interferences or the environment conditions such as fog, rain, and snow because of particles on the air reflecting multiple echoes [6], [7], [8], [9]. Fig. 1(a) shows a scenario of the received multiple echoes from rain drops once a single laser pulse is emitted [10]. Echo_3 is a valid information for detecting the distance from a target whereas echo_1, echo_2, and interference are undesired. Conventional LiDARs determine the distance information based on the first arrival echo_1 as can be seen in Fig. 1(b), which causes failure in extracting the distance information form the desired echo_3. Even though laser pulses with longer wavelength easily penetrate particle and mitigate this problem, interference from other sources or attacks cannot be avoided [11], [12].

The associate editor coordinating the review of this manuscript and approving it for publication was Khursheed Aurangzeb.

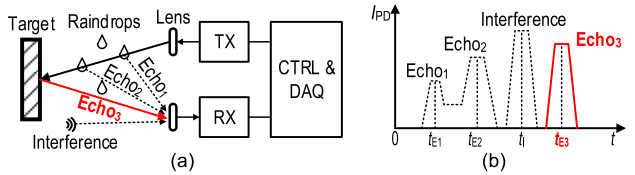

FIGURE 1. Conventional LiDAR system operating with multiple echoes and interference. (a) A scenario and (b) the timing information of received echoes.

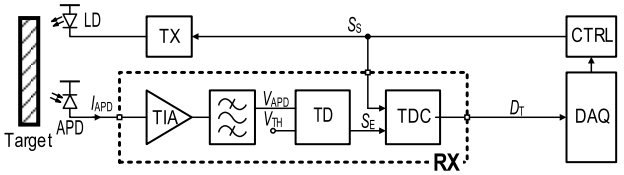

FIGURE 2. The basic block diagram of the conventional LiDARs.

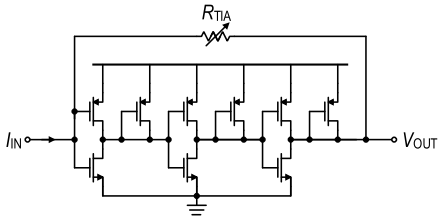

FIGURE 3. The circuit diagram of a conventional nonlinear TIA.

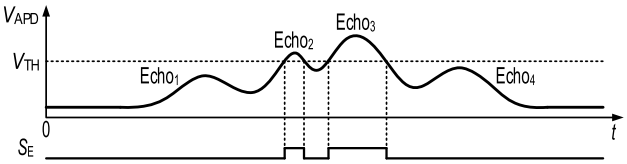

FIGURE 4. The timing diagram of the conventional TDs when multiple local peaks present.

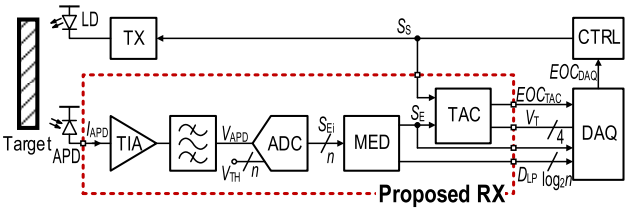

FIGURE 5. The block diagram of the proposed LiDAR.

Therefore, receiving instance and intensity information from multiple event and identifying the desired signal is critical to enhance robustness of pulsed LiDARs.

For detecting multiple events, several approaches have been developed [9], [13], [14]. In [13], multiple time-to-digital converters (TDCs) extract multiple events and store the distance information to a large memory which causes high area cost. Instead of using TDCs, multiple distance and intensity information can be extracted and stored using a time-to-amplitude converter (TAC) [14]. However, these schemes fail to extract multiple distance information when a received pulse includes multiple local peaks due to interferences or harsh environmental conditions. To avoid multiple local peaks received, sub-ns laser pulse and an on-chip avalanche photodiode (APD) is proposed in [9]. Nonetheless, this method cannot be compatible with conventional LiDARs with external APDs, and the wavelength of laser is limited due to the silicon-based integrated APD. To overcome these issues, a multi-event detecting pulsed LiDAR is proposed. Unlike conventional pulsed LiDARs, the proposed LiDAR can detect both multiple pulses and multiple local peaks in a pulse. Then, distance and intensity information is extracted for each pulse or peak.

II. PROPOSED LIDAR

A. CONVENTIONAL LIDARS

Fig. 2 shows a basic block diagram of the conventional LiDARs that consist of four main blocks: the analog front-end (AFE), time discriminator (TD), timing circuit (TC), and data acquisition (DAQ). When S_S sets high by a controller (CTRL), a laser diode in the transmitter TX emits light towards the target. The reflected light onto APD generates I_{APD} converted into voltage V_{APD} with a trans-impedance amplifier (TIA) followed by a band-pass filter (BPF) for noise reduction. Fig. 3 shows a conventional nonlinear 3-stage inverter-based TIA for high gain, high bandwidth, low noise, and low power consumption [15], [16], [17]. The gain of the TIA, R_{TIA}, can be controlled to adjust V_{APD} to an appropriate value. TD transforms the analog signal output into a digital end signal S_E suitable for time discrimination based on a threshold voltage V_{TH} [18], [19], [20], [21]. Then the time difference from start signal S_S and S_E is converted in to distance information with a TDC or TAC [22], [23], [24], [25]. However, conventional TDs cannot discriminate each local peak in a pulse with a single reference voltage in Fig. 4, where $echo_1$ and $echo_4$ are not detected. Multi-channel TDCs can be used to detect multiple echoes at the expense of increased hardware cost and power consumption. The most significant advantage of TAC over TDC is reduced hardware cost since multiple event detection can be implemented with a single TAC and a small multi-channel sample and hold (S&H) circuit [14].

B. DETAILS OF PROPOSED LIDAR

The proposed LiDAR detecting multiple event consists of a conventional nonlinear TIA, a BPF, a TD implemented by a flash ADC with n references, a multi-event detector (MED), a TAC, and a DAQ as shown in Fig. 5. The ADC generates n-bit end signal S_{Ei} with n references for multiple event detection. Unlike a conventional TD, the proposed TD allows for detecting multiple local peaks as depicted in Fig. 6.

Fig. 7(a) displays the block diagram of the MED that generates a stop signal S_E from n-bit S_{Ei}. The MED includes a rising and a falling edge detectors to generate edges of S_{Ei}. For the signals S_{RA} and S_{FA}, a short pulse is generated for each rising and falling edge of S_{Ei}, respectively, as can be

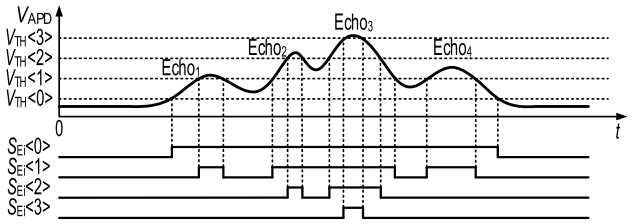

FIGURE 6. The timing diagram of the proposed TD with four references for detecting multiple local peaks.

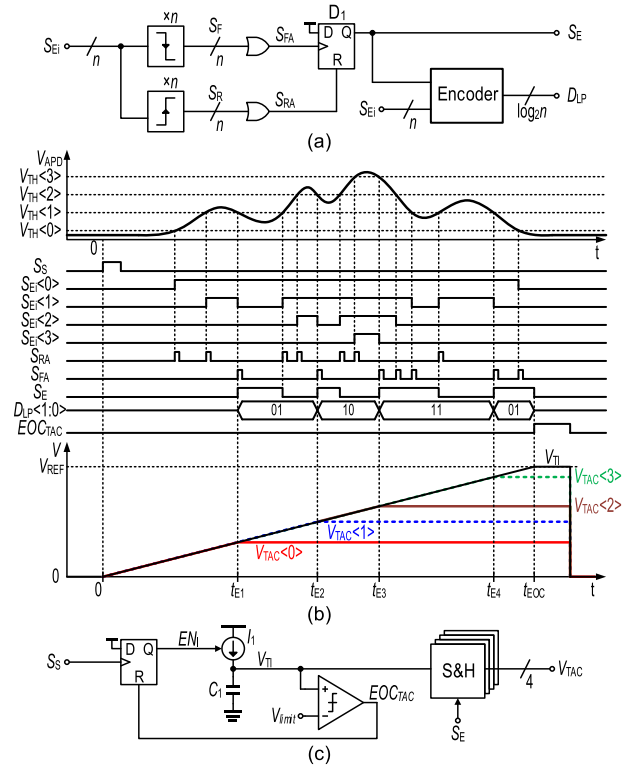

FIGURE 7. The proposed LiDAR ($n = 4$). (a) The block diagram of MED, (b) the timing diagram of MED and TAC, and (c) the block diagram of TAC.

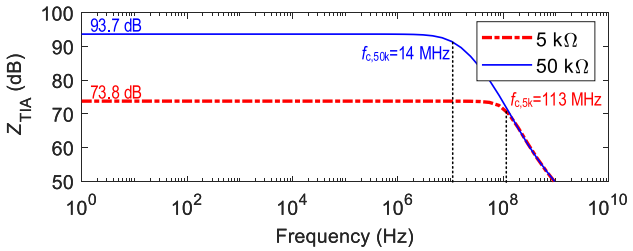

FIGURE 8. Simulation results about the gain of the proposed TIA.

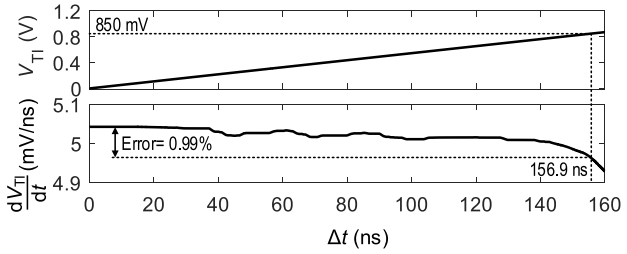

FIGURE 9. Simulation results about V_{TI} and the slope of V_{TI}.

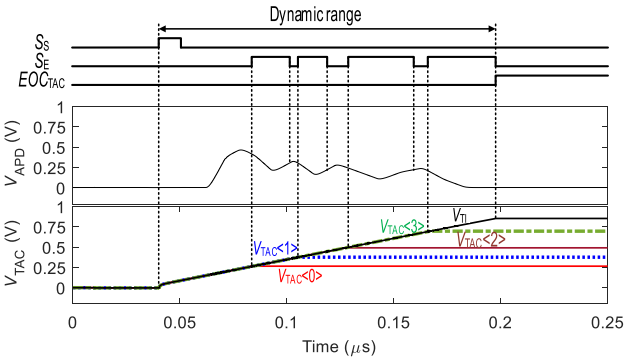

FIGURE 10. Simulation results about the timing diagram of the proposed LiDAR.

seen from Fig. 7(b). The signal S_E rises at the rising time of S_{FA} and falls at the rising time of S_{RA}, which indicates the time for each local peak at the rising edge of S_E. For intensity information at each local peak, $\log_2 n$-bit signal D_{LP} is extracted in a DAQ. Fig. 7(c) depicts the block diagram of the proposed TAC that stores the time information of up to four events based on each rising time of S_S and S_E. Once S_S rises, capacitor C_1 starts to charge based on DC current of I_1, which makes V_{TI} increases linearly in time. When S_E rises at t_{E1}, t_{E2}, t_{E3}, and t_{E4}, V_{TI} is sampled, held into 4-channel V_{TAC} with dedicated capacitors in the S&H block.

Since I_1 can be a function of V_{TI}, V_{TI} is limited to the voltage V_{limit} to guarantee the linearity of V_{TI}. When V_{TI} reaches V_{limit}, the comparator enables the end-of-conversion signal EOC_{TAC} and proceeds the operations of DAQ in Fig. 5. Then the distance information in the four-channel V_{TAC} is digitized, and $\log_2 n$-bit intensity data D_{LP} are deliver to the output with V_{TAC} for each local peak or pulse.

III. SIMULATION RESULTS

Cadence Spectre with TSMC 0.18 μm process parameters was used for SPICE simulation with a 1.8 V power supply. Fig. 8 shows the frequency response of the 3-stage inverter-based TIA in Fig. 3 with 3 pF input capacitance. The gain of TIA is obtained as 73.8 and 93.7 dB by changing the value of R_{TIA} to either 5 or 50 kΩ, where their cut-off frequency is obtained as 113 and 14 MHz, respectively.

To quantify the range of linear working range of V_{TI}, the simulation results of V_{TI} and the derivative of V_{TI} in terms of time are shown in Fig. 9. Since dV_{TI}/dt drops as time goes on, the nonlinearity increases and thus the distance information can be degraded. At the starting point $t = 0$, dV_{TI}/dt is obtained as 5.04 mV/ns. V_{limit} is set to 850 mV for the dV_{TI}/dt drop of 1%, where the dynamic range of the proposed TAC is 156.9 ns. Fig. 10 shows the transient simulation results of the

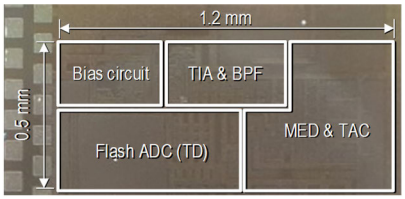

FIGURE 11. Micrograph of the proposed LiDAR.

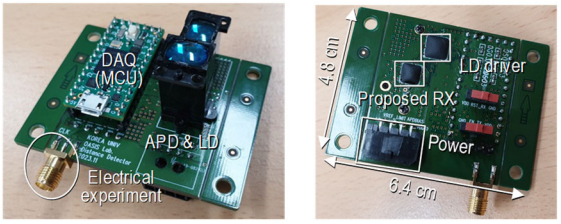

FIGURE 12. Experimental setup of the proposed LiDAR.

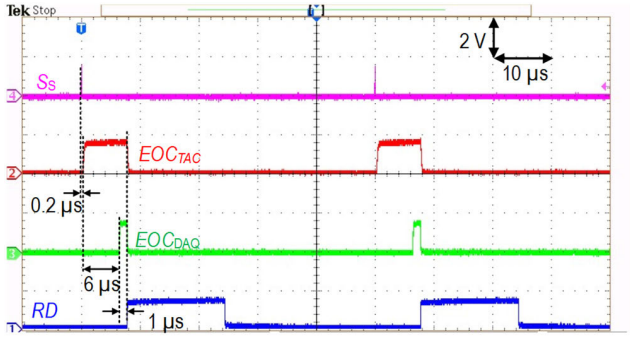

FIGURE 13. Experimental results of transient digital outputs.

proposed TAC with four multiple events. When S_S goes high, four channel of V_{TAC} is obtained based on the given profile of V_{APD}.

IV. EXPERIMENTAL RESULTS

The proposed LiDAR is fabricated in TSMC 0.18 μm CMOS technology with a 1.8 V power supply. The micrograph of the proposed LiDAR is shown in Fig. 11, where the active area is approximately 0.5×1.2 mm^2. To reduce the delay caused by wire bonding, the proposed LiDAR involves mounting both the receiver and a laser diode driver on a single prototype printed circuit board (PCB) as shown in Fig. 12. The proposed LiDAR receives the reflected light from an object once laser diode LD emits pulsed light. The time delay and the intensity of reflected light associated with this process are extracted for each event.

Fig. 13 shows experimental results for the digital outputs of the proposed LiDAR with signals S_S, EOC_{TAC}, EOC_{DAQ}, and the read signal *RD*. The proposed LiDAR incorporates with and micro-controller unit (MCU) as a DAQ with a 10-bit ADC. S_S rises for sampling every 50 μs. 0.2 μs after the light emission, the sampling for event detection is finished just before the rising edge of EOC_{TAC}. Then digitization for

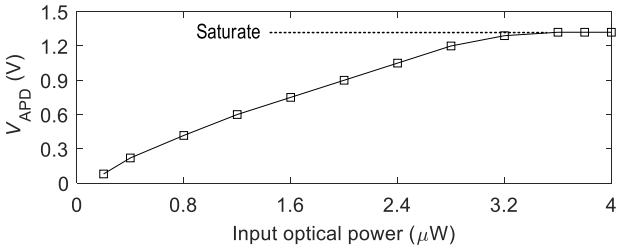

FIGURE 14. Experimental results for quantifying the TIA based on optical input power.

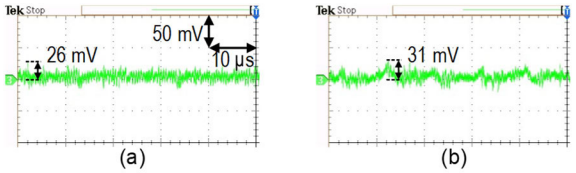

FIGURE 15. Measured peak noise of V_{APD} when R_{TIA} is set to (a) 5 and (b) 50 KΩ.

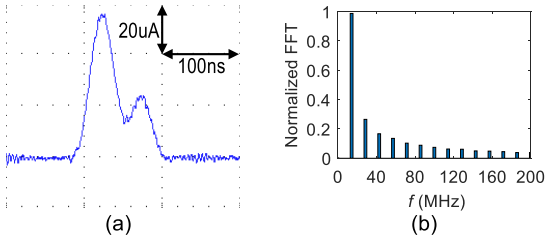

FIGURE 16. Experimental results for generating multiple events with water droplets on a glass between an object and the receiver. (a) The waveform of diode current with two events and (b) its fast Fourier transform.

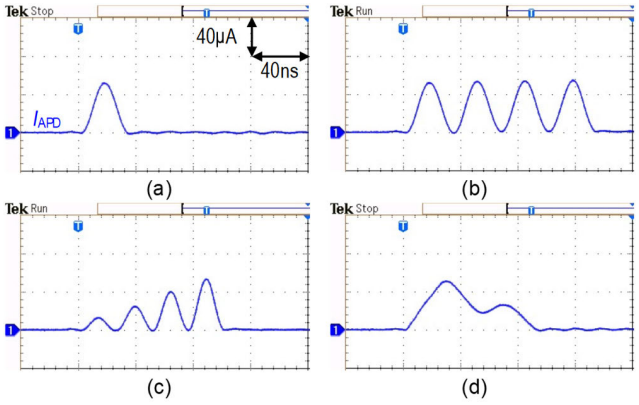

FIGURE 17. Several input APD currents used in experiment and measured V_{APD}. (a) 1 echo, (b) 4 echoes, (c) amplitude-increasing 4 echoes, and (d) mimicked 2 local peaks.

the distance information is conducted until the rising edge of EOC_{DAQ}, which takes 6 μs. When the read signal RD rises after EOC_{DAQ} enables, the distance and intensity information is ready for the final output.

The measured characteristic of the TIA according to the input optical power is shown in Fig. 14, where the gain

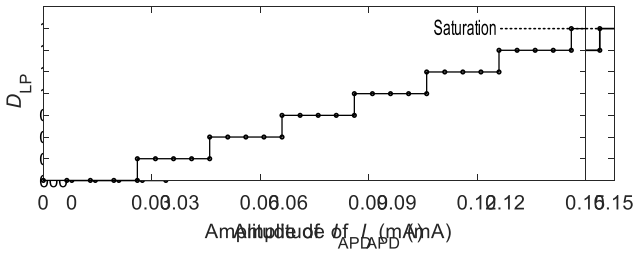

FIGURE 18. Experimental results about the digital code D_{LP} for the intensity information.

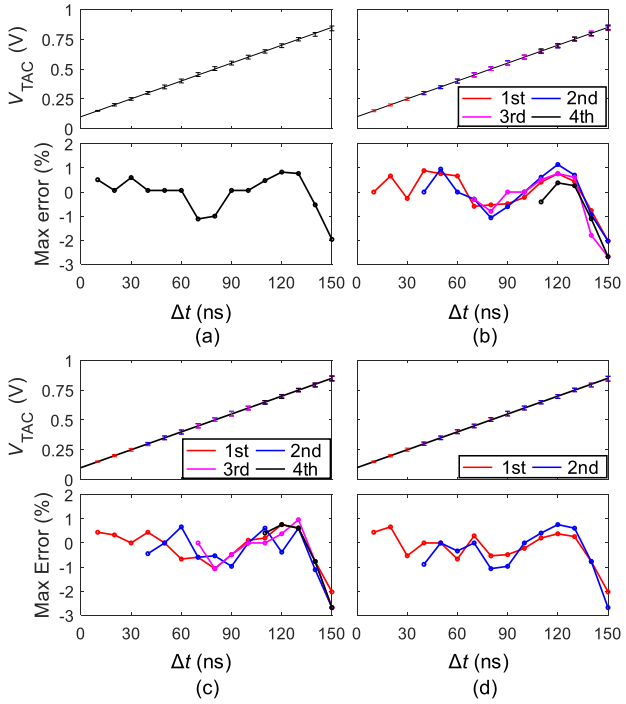

FIGURE 19. Experimental results of the TAC output V_{TAC} and maximum error of V_{TAC} when the input shape is (a) 1 echo, (b) 4 echoes, (c) amplitude-increasing 4 echos, and (d) mimicked 2 local peaks.

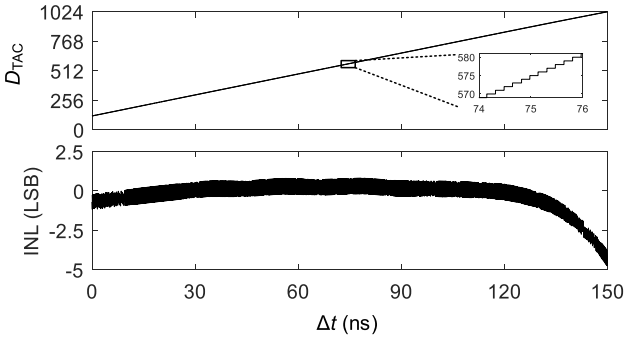

FIGURE 20. Experimental results about the digital code D_T for the time information generated by DAQ and the INL of D_{TAC}.

TABLE 1. Measured performance of the proposed LiDAR.

	Case 1	Case 2
Dynamic range (ns)	120	150
Dynamic range (m)	18	22.5
Maximum error (%)	1.12	2.68

TABLE 2. Performance summary and comparison of LiDARs.

	This work	2012 [13]	2018 [14]	2019 [9]	2023 [26]
Technology (nm)	180	350	180	180	180
Timing circuit	TAC	TDC	TAC	TDC	TDC
APD	off-chip	off-chip	off-chip	on-chip	on-chip
Intensity detection	**Y**	N	**Y**	N	N
Multi-event detection	**Y**	**Y**	**Y**	**Y**	N
Multi-local peak detection	**Y**	N	N	N	N
Dynamic range (m)	22.5	9	120	10	2.7
Resolution (ps)	146.5	144	N/A	10	1,000
Chip area (mm^2)	0.60	N/A	0.01	2.20	0.227

of the APD is 50 A/W at 905 nm wavelength. Fig. 15 shows the measurement results of the peak noise, which is approximately 26 mV and 31 mV as R_{TIA} is set to 5 k and 50 kΩ, respectively. For quantification of the proposed LiDAR under the multiple event conditions, experiments are conducted to obtain an electrical model by putting water droplets on a glass between an object and the proposed LiDAR as shown in Fig. 16(a). The external APD modeled C30737 generates the current profile of I_{APD} from the 905 nm laser diode pulse with its width of 50 ns. Fig. 16(b) illustrates the frequency analysis using fast Fourier transform, where the dominant frequency of I_{APD} appears at around 14.4 MHz. The electrical models of I_{APD} used in this experiment are generated by using a function generator as followed: Fig. 17(a) represents a single event of sine-shaped pulse. Four pulses with equal shape are modeled as multiple events in Fig. 17(b). Four pulses with unequal amplitude are modeled in Fig. 17(c). Lastly, Fig. 17(d) mimicked I_{APD} from Fig. 16(a).

Fig. 18 displays experimental results for the 3-bit amplitude information based on the single pulse electrical input shows that LSB step increases every 20 μA. If the current goes beyond 146 μA, the amplitude output is saturated to its maxim value. To investigate the linearity of the proposed TAC, Fig. 19 depicts the time difference between the rising edges of S_S and S_E, Δt, varied up to 150 ns corresponding to 22.5 m in distance at V_{limit} = 850 m. Each Δt is conducted 20 iterations, and error bar with their minimum and maximum values are depicted. The maximum error indicates the maximum voltage difference between the fitted line and the actual voltage output V_{TAC} out of 20 iterations, where each plot is extracted based on the electrical input from Fig. 17. As a result, the maximum absolute errors for the dynamic range is limited to 120 and 150 ns are 1.12% and 2.68%, respectively. Fig. 20 shows the experimental results regarding the output of 10-bit DAQ with the input of Fig. 17(a) while varying Δt from 0 to 150 ns. The integral non-linearity (INL) of D_{TAC} is in good accordance with the linearity error in Fig. 19(a). The worst-case INL becomes

−1.17 and −4.74 LSBs for the dynamic range is limited to 120 and 150 ns, respectively. The summary is presented in Table 1 through experimental results. Table 2 compares the performance of the proposed LiDAR with the previously published works. The proposed LiDAR reduces complexity and chip area by using a TAC, and enables a multi-local peak detection. The performance of the proposed LiDAR is suitable for medium-range LiDAR applications with the intensity and distance information of the multiple events and multiple local peaks caused by external interference and the harsh environment conditions.

V. CONCLUSION

This paper presents a robust multi-event detecting LiDAR that extracts intensity and distance information for up to four events caused from external interference and harsh environmental conditions. At the expense of additional S&H circuits, more events can be detected. The integration of a TAC in the proposed LiDAR offers advantages of detecting multiple local peaks with less hardware complexity and reducing the need for additional memory circuits. Since the proposed LiDAR enhances the reliability of multiple echo detection, it can be used for side monitoring LiDAR of a vehicle. Also, the proposed LiDAR can be a suitable tool in fields such as traffic condition detection, obstacle avoidance, and environmental awareness. However, the proposed method for detecting multiple events can also be used for long range applications.

REFERENCES

[1] B. Behroozpour, P. A. M. Sandborn, M. C. Wu, and B. E. Boser, "LiDAR system architectures and circuits," *IEEE Commun. Mag.*, vol. 55, no. 10, pp. 135–142, Oct. 2017.

[2] T. Raj, F. H. Hashim, A. B. Huddin, M. F. Ibrahim, and A. Hussain, "A survey on LiDAR scanning mechanisms," *Electronics*, vol. 9, no. 5, p. 741, Apr. 2020.

[3] R. Roriz, J. Cabral, and T. Gomes, "Automotive LiDAR technology: A survey," *IEEE Trans. Intell. Transp. Syst.*, vol. 23, no. 7, pp. 6282–6297, Jul. 2022.

[4] G. Chen, C. Wiede, and R. Kokozinski, "Data processing approaches on SPAD-based d-TOF LiDAR systems: A review," *IEEE Sensors J.*, vol. 21, no. 5, pp. 5656–5667, Mar. 2021.

[5] H. Seo, H. Yoon, D. Kim, J. Kim, S.-J. Kim, J.-H. Chun, and J. Choi, "Direct TOF scanning LiDAR sensor with two-step multievent histogramming TDC and embedded interference filter," *IEEE J. Solid-State Circuits*, vol. 56, no. 4, pp. 1022–1035, Apr. 2021.

[6] A. Haider, M. Pigniczki, M. H. Köhler, M. Fink, M. Schardt, Y. Cichy, T. Zeh, L. Haas, T. Poguntke, M. Jakobi, and A. W. Koch, "Development of high-fidelity automotive LiDAR sensor model with standardized interfaces," *Sensors*, vol. 22, no. 19, p. 7556, Oct. 2022.

[7] T. Fahey, M. Islam, A. Gardi, and R. Sabatini, "Laser beam atmospheric propagation modelling for aerospace LiDAR applications," *Atmosphere*, vol. 12, no. 7, p. 918, Jul. 2021.

[8] A. Haider, M. Pigniczki, S. Koyama, M. H. Köhler, L. Haas, M. Fink, M. Schardt, K. Nagase, T. Zeh, A. Eryildirim, T. Poguntke, H. Inoue, M. Jakobi, and A. W. Koch, "A methodology to model the rain and fog effect on the performance of automotive LiDAR sensors," *Sensors*, vol. 23, no. 15, p. 6891, Aug. 2023.

[9] M. Hintikka and J. Kostamovaara, "Experimental investigation into laser ranging with sub-ns laser pulses," *IEEE Sensors J.*, vol. 18, no. 3, pp. 1047–1053, Feb. 2018.

[10] M. Rodríguez-Cortina, P. Adamiec, J. Barbero, X. Quintana, and M. A. Geday, "Emulation technique of multiple overlapped return echoes of a spatial LiDAR with 100-dB dynamic resolution," *IEEE Trans. Instrum. Meas.*, vol. 70, pp. 1–7, 2021.

[11] H. Xia, G. Shentu, M. Shangguan, X. Xia, X. Jia, C. Wang, J. Zhang, J. S. Pelc, M. M. Fejer, Q. Zhang, X. Dou, and J.-W. Pan, "Long-range micro-pulse aerosol LiDAR at 1.5 μm with an upconversion single-photon detector," *Opt. Lett.*, vol. 40, no. 7, pp. 1579–1582, 2015.

[12] Y. Miao, H. Lin, B. Li, T. Dong, C. He, J. Du, X. Zhao, Z. Zhou, J. Su, H. Wang, Y. Dong, B. Lu, L. Dong, and H. H. Radamson, "Review of Ge(GeSn) and InGaAs avalanche diodes operating in the SWIR spectral region," *Nanomaterials*, vol. 13, no. 3, p. 606, Feb. 2023.

[13] S. Kurtti and J. Kostamovaara, "An integrated receiver channel for a laser scanner," in *Proc. IEEE Int. Instrum. Meas. Technol. Conf.*, May 2012, pp. 1358–1361.

[14] H.-J. Kim, E.-G. Lee, and C.-Y. Kim, "A high-multi target resolution focal plane array-based laser detection and ranging sensor," *Sensors*, vol. 19, no. 5, p. 1210, Mar. 2019.

[15] T.-H. Ngo, C.-H. Kim, Y. J. Kwon, J. S. Ko, D.-B. Kim, and H.-H. Park, "Wideband receiver for a three-dimensional ranging LADAR system," *IEEE Trans. Circuits Syst. I, Reg. Papers*, vol. 60, no. 2, pp. 448–456, Feb. 2013.

[16] H. Zheng, R. Ma, M. Liu, and Z. Zhu, "A linear-array receiver analog front-end circuit for rotating scanner LiDAR application," *IEEE Sensors J.*, vol. 19, no. 13, pp. 5053–5061, Jul. 2019.

[17] X. Wang, R. Ma, D. Li, H. Zheng, M. Liu, and Z. Zhu, "A low walk error analog front-end circuit with intensity compensation for direct ToF LiDAR," *IEEE Trans. Circuits Syst. I, Reg. Papers*, vol. 67, no. 12, pp. 4309–4321, Dec. 2020.

[18] H.-S. Cho, C.-H. Kim, and S.-G. Lee, "A high-sensitivity and low-walk error LADAR receiver for military application," *IEEE Trans. Circuits Syst. I, Reg. Papers*, vol. 61, no. 10, pp. 3007–3015, Oct. 2014.

[19] H. Zheng, R. Ma, M. Liu, and Z. Zhu, "High sensitivity and wide dynamic range analog front-end circuits for pulsed TOF 4-D imaging LADAR receiver," *IEEE Sensors J.*, vol. 18, no. 8, pp. 3114–3124, Apr. 2018.

[20] Y. K. Moon, Y. B. Shim, and H. K. Song, "Error correction technique of distance measurement for ToF LiDAR sensor," *KSII Trans. Internet Inf. Syst.*, vol. 12, no. 2, Feb. 2018.

[21] H. Zheng, R. Ma, X. Wang, M. Liu, and Z. Zhu, "A CMOS peak detect and hold circuit with auto-adjust charging current for NS-scale pulse ToF LiDAR application," *IEEE Trans. Circuits Syst. I, Reg. Papers*, vol. 67, no. 12, pp. 4409–4419, Dec. 2020.

[22] K. Cui, J. Yu, J. Zou, and X. Li, "A high-resolution TDC design based on multistep fine time measurement by utilizing delay-adjustable looped carry chains on FPGAs," *IEEE Trans. Instrum. Meas.*, vol. 72, pp. 1–10, 2023.

[23] C.-C. Wang, K.-Y. Chao, S. Sampath, and P. Suresh, "Anti-PVT-variation low-power time-to-digital converter design using 90-nm CMOS process," *IEEE Trans. Very Large Scale Integr. (VLSI) Syst.*, vol. 28, no. 9, pp. 2069–2073, Sep. 2020.

[24] C. Piao, Y. Ahn, D. Kim, J. Park, J. Kang, M. Shin, K. Seo, S.-J. Kim, J.-H. Chun, and J. Choi, "A 70 mW indirect time-of-flight image sensor with depth dynamic range enhancement and fixed depth noise compensation," in *Proc. IEEE Asian Solid-State Circuits Conf. (A-SSCC)*, Nov. 2021, pp. 1–3.

[25] M. Zhang, C.-H. Chan, Y. Zhu, and R. P. Martins, "3.5 A 0.6 V 13b 20MS/s two-step TDC-assisted SAR ADC with PVT tracking and speed-enhanced techniques," in *IEEE Int. Solid-State Circuits Conf. (ISSCC) Dig. Tech. Papers*, San Francisco, CA, USA, Feb. 2019, pp. 66–68.

[26] J.-E. Joo, S. Choi, Y. Chon, and S.-M. Park, "A low-cost measurement methodology for LiDAR receiver integrated circuits," *Sensors*, vol. 23, no. 13, p. 6002, Jun. 2023.

SEUNG SOO KWAK (Graduate Student Member, IEEE) received the B.S. degree in electrical engineering from Korea University, Seoul, South Korea, in 2017, where he is currently pursuing the unified degree in electrical engineering. His research interests include power management, energy harvesting, electronics in vehicles, LiDAR, and ToF sensor IC.

JISEONG LEE (Graduate Student Member, IEEE) received the B.S. degree in electrical engineering from the Kumoh National Institute of Technology, Gumi, South Korea, in 2018. He is currently pursuing the M.S. and Ph.D. degrees with Korea University, Seoul, South Korea. He received American Engineering Experiential Work with Purdue University, in 2016. His research interests include current regulators for system-on-chip (SoC) applications, dc/dc control techniques, low-power switched mode power supplies, and power management ICs.

YUN CHAN IM (Graduate Student Member, IEEE) received the B.S. degree in electrical engineering from Korea University, Seoul, South Korea, in 2018, where he is currently pursuing the M.S. and Ph.D. degrees. His research interests include energy harvesting systems for wireless sensor networks, low-power switched-mode power supplies, and power management ICs.

HYUNJIN LEE (Graduate Student Member, IEEE) received the B.S. degree in electronic and information engineering from Korea University, Sejong Campus, in 2020. She is currently pursuing the M.S. and Ph.D. degrees with Korea University, Seoul Campus. Her research interests include data converters, sensor ICs, and image sensor systems for time-of-flight (TOF) sensors.

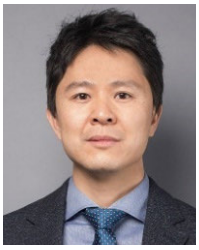

YONG SIN KIM (Senior Member, IEEE) received the B.S. and M.S. degrees in electronics from Korea University, Seoul, South Korea, in 1999 and 2003, respectively, and the Ph.D. degree in electrical engineering from the University of California at Santa Cruz, Santa Cruz, CA, USA, in 2008. From 2008 to 2012, he was with the University of California Advanced Solar Technologies Institute (UC Solar), where he researched on optimizing power in distributed photovoltaic systems. From 2012 to 2014, he was with the School of Electrical and Electronics Engineering, Chung-Ang University, Seoul, where he was involved in the development of sensors for human–machine interfaces. Since March 2014, he has been with the School of Electrical Engineering, Korea University. His current research interests include the cross-disciplinary integration of circuits and systems for energy harvesting and sensor applications.